Title: Imaging transcriptomics: Convergent cellular, transcriptomic, and molecular neuroimaging signatures in the healthy adult human brain

Daniel Martins[1#*], Alessio Giacomel[1#], Steven CR Williams[1], Federico Turkheimer[1], Ottavia Dipasquale[1#], Mattia Veronese[1,2#*], and *PET templates working group*

[1]Department of Neuroimaging, Institute of Psychiatry, Psychology and Neuroscience, King's College London, De Crespigny Park, London SE5 8AF, UK

[2]Department of Information Engineering, University of Padua, Italy

[#]Equal contribution

***Corresponding authors:**

Daniel Martins, MD PhD & Mattia Veronese, PhD

Department of Neuroimaging,

Institute of Psychiatry, Psychology and Neuroscience, King's College London

De Crespigny Park, London SE5 8AF, United Kingdom

Emails : daniel.martins@kcl.ac.uk; mattia.veronese@kcl.ac.uk

Telephone: +44 (0)2032283064

Category of manuscript

Original research

Abstract

The expansion of neuroimaging techniques over the last decades has opened a wide range of new possibilities to characterize brain dysfunction in several neurological and psychiatric disorders. However, the lack of specificity of most of these techniques, such as magnetic resonance imaging (MRI)-derived measures, to the underlying molecular and cellular properties of the brain tissue poses limitations to the amount of information one can extract to inform precise models of brain disease. The integration of transcriptomic and neuroimaging data, known as 'imaging transcriptomics', has recently emerged as an indirect way forward to test and/or generate hypotheses about potential cellular and transcriptomic pathways that might underly specific changes in neuroimaging MRI biomarkers. However, the validity of this approach is yet to be examined in-depth. Here, we sought to bridge this gap by performing imaging transcriptomic analyses of the regional distribution of well-known molecular markers, assessed by positron emission tomography (PET), in the healthy human brain. We focused on tracers spanning different elements of the biology of the brain, including neuroreceptors, synaptic proteins, metabolism, and glia. Using transcriptome-wide data from the Allen Brain Atlas, we applied partial least square regression to rank genes according to their level of spatial alignment with the regional distribution of these neuroimaging markers in the brain. Then, we performed gene set enrichment analyses to explore the enrichment for specific biological and cell-type pathways among the genes most strongly associated with each neuroimaging marker. Overall, our findings show that imaging transcriptomics can recover plausible transcriptomic and cellular correlates of the regional distribution of benchmark molecular imaging markers, independently of the type of parcellation used to map gene expression and neuroimaging data. Our data support the plausibility and robustness of imaging transcriptomics as an indirect approach for bridging gene expression, cells and macroscopical neuroimaging and improving our understanding of the biological pathways underlying regional variability in neuroimaging features.

Keywords: Imaging transcriptomics; Allen Brain Atlas; transcriptomics; positron tomography emission.

Introduction

Over the past two decades, in-vivo human neuroimaging techniques, such as magnetic resonance imaging (MRI), have emerged as powerful tools to advance our understanding of macroscopic neural phenotypes measured across the entire brain[1]. The increasing application of MRI for studying neurological and psychiatric disorders has provided detailed anatomical characterizations of regional patterns of brain's structural and functional alterations in these disorders[2,3]. However, the lack of specificity of most MRI-based techniques to the underlying molecular and cellular properties of the brain tissue[4] has limited the potential of these neuroimaging biomarkers to inform mechanistic models of brain disease, understand biological mechanisms behind regional vulnerability to pathological changes or identify biological pathways that might be amenable to pharmacological intervention.

The recent introduction of comprehensive, brain-wide gene expression atlases such as the Allen Human Brain Atlas (AHBA) has opened new opportunities for understanding how spatial variations on the molecular transcriptomic scale relate to the macroscopic neuroimaging phenotypes[5,6]. This unprecedented capacity to link molecular pathways to macroscale brain organization has given rise to the emergent field of imaging transcriptomics[7]. Imaging transcriptomics is concerned with the identification of spatial correlations between gene expression patterns and some property of brain structure or function, as measured by neuroimaging[7]. The main goal of this approach is to identify genes with spatial profiles of regional expression that track anatomical variations in a certain neuroimaging biomarker. Typically, these analyses include mapping both gene expression data from the AHBA and neuroimaging maps to a common neuroimaging space (e.g., parcellated atlas of the brain). Then, one or multiple neuroimaging biomarkers (response variables) are related to expression measures of several thousands of genes in each region (predictor variables), often by using multivariate statistical techniques such as partial least square regression (PLS). As a result, genes are ranked according to the degree of spatial alignment of their expression with the neuroimaging biomarker under exam. An enrichment analysis is then performed on the top-ranking genes: when a significant number of top-ranking genes have a particular gene annotation (e.g., biological or molecular pathway) relative to the number of annotations present in a reference set (e.g., the entire genome), then the top-ranking genes are said to be enriched for that annotation. Because the top-ranking genes are strongly associated with the brain map of interest, the enriched annotations are used as an indirect way to test and generate hypotheses about the potential cellular and biological pathways that might underly specific neuroimaging features[7]. This approach has already begun to provide insights into how regional variations in gene expression relate to diverse properties of brain structure[8-13] and function[14-20], changes during brain disease[21-31] or development[32-34].

As the field develops, it is important, on the one side, to establish methodological guidelines to ensure consistent and reproducible results; and, on the other side, to examine the validity of this approach to capture indirect associations between gene expression, cells and macroscopical neuroimaging features. Recent efforts focusing on the first aspect have provided key tools and practical guides for the implementation of these analyses[7,35-37], while the second aspect on validity is yet to be assessed in-depth. To the best of our knowledge, only two previous works have examined it within a limited scope. In both studies, maps of the mean expression of sets of genes related to oligodendrocytes were found to be positively correlated with MRI measures sensitive to myelin (i.e magnetization transfer ratio or T1W/T2W ratio)[8,31]. Whether imaging transcriptomics can also successfully recover plausible

transcriptomic and cellular correlates of the regional distribution of neuroimaging biomarkers beyond those related to myelin is currently elusive.

In this work, we sought to bridge this gap by performing imaging transcriptomic analyses of the regional distribution of well-known molecular markers (as assessed by positron emission tomography, PET) in the healthy human brain. Thanks to a large collaborative effort, we could examine a vast number of tracers spanning different elements of the biology of the brain, including neuroreceptors, synaptic proteins, metabolism, and glia. While most PET tracers do not necessarily have binding affinity for a single specific brain cell-type or biological pathway, departing from a molecular neuroimaging phenotype where the target is known allows for a more precise generation of hypotheses regarding pathways that should be captured by imaging transcriptomics if the approach is valid (see Table 1 for a summary of all markers used and our respective *a priori* specific hypotheses regarding biological and cell-type pathways enrichment).

Table 1. List of neuroimaging markers and respective hypotheses. In this table, we present a summary of all neuroimaging markers used in our transcriptomics analyses and the respective *a priori* hypotheses we formulated in respect to the biological and cellular pathways that we expected to align with the regional distribution of each tracer.

Domain	Marker	Main target	Hypothesis
Neuroreceptors, synaptic proteins and metabolism	[^{11}C]Flumazenil	$GABA_A$ receptor	Alignment with the regional distribution of genes involved in synaptic structure and neurotransmission, which are highly expressed in populations of neuronal cells.
	[^{18}F]GE179	NMDA receptor	
	[^{11}C]UCB-J	Synaptic vesicle glycoprotein 2A (SV2A)	
	[^{18}F]FDG	Fluorodeoxyglucose (metabolic activity)	
Astroglia and myelin	[^{11}C]BU99008	Imidazoline$_2$ binding site (I_2BS)	Alignment with the regional distribution of astrocytic genes.
	L-[^{11}C]deprenyl-D2	Monoamine oxidase B (MAO-B)	
	Magnetization transfer ratio (MT)	Sensitive to myelin (including intra-cortical myelination)	Alignment with the regional distribution of oligodendrocytes and oligodendrocyte precursor cells.
	Myelin Water Content (WC)	Sensitive to myelin (including intra-cortical myelination)	
18-kDa Translocator protein (TSPO) and cyclooxygenase (Cox)	[^{11}C]PK11195	TSPO (first-generation)	Alignment with the regional distribution of genes of the neuroimmune response axis (microglia/astrocytes).
	[^{18}F]DPA174	TSPO (second-generation)	
	[^{11}C]PBR28		
	[^{11}C]ER176		
	[^{11}C]PS13	COX-1	

Methods

Neuroimaging data. We capitalized on collaborations with several research groups (also referred as "PET templates working group") to gather a large pool of templates of different PET tracers, including: [^{11}C]Flumazenil[38], [^{18}F]GE179[39], [^{11}C]UCB-J (unpublished data), [^{18}F]FDG (unpublished data), [^{11}C]BU99008[40], L-[^{11}C]deprenyl-D2[41], [^{11}C]PK11195[42], [^{18}F]DPA174 (unpublished), [^{11}C]PBR28[43], [^{11}C]ER176[44] and [^{11}C]PS13[45]. For each tracer, neuroimaging templates were created as average maps from independent sets of healthy controls (number of subjects ranging from 7 to 38). Data were acquired with different experimental design protocols and quantified in accordance to the best PET imaging practice for each of these radioligands, as described in the respective original studies. We also included two maps from MRI measures sensitive to myelin, namely a map of magnetization transfer ratio (MT) [46] and one of myelin water content (WC)[47] for comparison with previous studies. For details on the samples, data acquisition and quantification and voxel-wise maps of each tracer please see Supplementary.

For each neuroimaging marker, we calculated the mean distribution within each of the 83 regions-of-interest of the Desikan-Killiany[48] (DK) atlas by using the FMRIB software library (FSL, v6)[49]. Then, we calculated pairwise Pearson's correlations between the normalised regional distribution of each pair of markers, assessing the significance of each pair-wise correlation by using tests that account for the inherent spatial autocorrelation of the data (see section below on spatial permutation testing) (Supplementary Figure S1).

In Figure 1 we provide a summary of our full imaging transcriptomics analysis pipeline (Figure 1), which we describe in detail below.

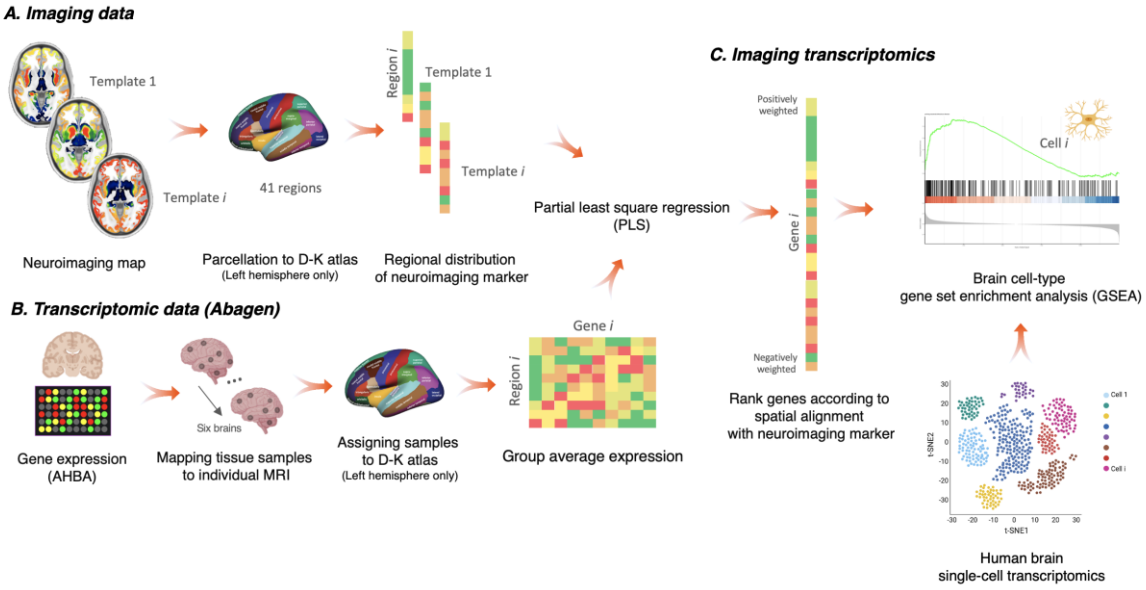

Figure 1. Imaging transcriptomics pipeline. (A) For each neuroimaging marker, we calculated the average distribution within each of the 83 regions-of-interest of the Desikan-Killiany (DK) atlas; only the data from the left hemisphere was used for further analyses since the Allen Human Brain Atlas only includes data from the right hemisphere for two subjects; (B) Gene expression analysis. We used *abagen* to obtain gene expression profiles from the AHBA in the 41 regions of the DK atlas (left hemisphere) across the six post-mortem brains sampled in this atlas. We excluded all genes with normalized expression values below the background (15,633 genes met this criterion). When more than one probe was available for

a certain gene, we selected the probe with the highest consistency in expression across the 6 donors. We used partial least squares regression (PLS) to rank all genes according to their association with the regional distribution of each neuroimaging marker. Finally, we performed gene set enrichment analyses for gene ontologies and genes expressed in different cell-types (using single cell transcriptomic data from the human brain, as derived from previous studies). The gene set enrichment analyses were implemented with WebGestalt.

Transcriptomic data. Regional microarray expression data were obtained from six post-mortem brains as part of the AHBA (http://human.brain-map.org/) (ages 24–57 years)[50]. We used the *abagen* toolbox (https://github.com/netneurolab/abagen) to process and map the transcriptomic data onto the 83 parcellated brain regions from the DK atlas. Briefly, genetic probes were reannotated using information provided by *Arnatkeviciute et al., 2019*[7] instead of the default probe information from the AHBA dataset, hence discarding probes that cannot be reliably matched to genes. Following previously published guidelines for probe-to-gene mappings and intensity-based filtering[7], the reannotated probes were filtered based on their intensity relative to background noise level; probes with intensity lower than the background in ≥50% of samples were discarded. A single probe with the highest differential stability (highest pooled correlation across donors) was selected to represent each gene[51]. This procedure retained 15,633 probes, each representing a unique gene.

Next, tissue samples were assigned to brain regions using their corrected MNI coordinates (https://github.com/chrisfilo/alleninf) by finding the nearest region within a radius of 2 mm. To reduce the potential for misassignment, sample-to-region matching was constrained by hemisphere and cortical/subcortical divisions. If a brain region was not assigned to any sample based on the above procedure, the sample closest to the centroid of that region was selected to ensure that all brain regions were assigned a value. Samples assigned to the same brain region were averaged separately for each donor. Gene expression values were then normalized separately for each donor across regions using a robust sigmoid function and rescaled to the unit interval. We applied this procedure for cortical and subcortical regions separately, as suggested by *Arnatkeviciute et al., 2019*[7]. Scaled expression profiles were finally averaged across donors, resulting in a single matrix with rows corresponding to brain regions and columns corresponding to the retained 15,633 genes. As a further robustness test, we conducted leave-one-donor out sensitivity analyses to generate six expression maps containing gene expression data from all donors, one at a time. The principal components of these six expression maps were highly correlated (average Pearson's correlation of 0.993), supporting the idea that our final gene expression maps where we averaged gene expressions for each region across the six donors is unlikely to be biased by data from a specific donor. Since the AHBA only includes data for the right hemisphere for two subjects we only considered the 41 regions of left hemisphere regions (34 cortical plus 7 subcortical regions) for the following analyses.

Partial least square regression. Partial least square regression uses the gene expression measurements (the predictor – or independent – variables) to predict regional variation in neuroimaging features (the response – or dependent – variables). This approach allows us to rank all genes by their multivariate spatial alignment with the regional distribution of each neuroimaging feature, while accounting for inherent collinearity in the predictor variables due to

gene co-expression. The first PLS component (PLS1) is the linear combination of the weighted gene expression scores that have a brain expression map that covaries the most with the neuroimaging map. As the components are calculated to explain the maximum covariance between dependent and independent variables, the first component does not necessarily need to explain the maximum variance in the dependent variable. Of note, as the number of PLS components calculated increases, the amount of variance explained by each of them progressively decreases. Here, we examined models across a range of components (between 1 and 15) and evaluated the relative variance explained by each component against 1,000 null models, where we preserved the spatial autocorrelation of the data (see the section 'spatial permutation test' for more details). We then moved to further analyses only the PLS component explaining the largest amount of variance, which in our case was always the first component (PLS1). The error in estimating each gene's PLS1 weight was assessed by bootstrapping (resampling with replacement of the 41 brain regions), and the ratio of the weight of each gene to its bootstrap standard error was used to calculate the *Z* scores and, hence, rank the genes according to their contribution to the PLS component under investigation[52]. Genes with large positive PLS weights correspond to genes that have higher than average expression in regions where the neuroimaging biomarker has a higher distribution, and lower than average expression in regions where the biomarker has a lower distribution. Mid-rank PLS weights showed expression gradients that are weakly related to the pattern of regional distribution of the neuroimaging biomarker. On the other side, genes with large negative PLS weights correspond to genes that have higher than average expression in regions where neuroimaging biomarker is lowly distributed, and lower than average expression in regions where the biomarker is highly distributed. Since in our analyses we were mostly interested in genes that track the distribution of each neuroimaging biomarker (i.e., that correlate positively with the biomarker), we focused on genes with positive PLS weights (even if we also present the results for genes with negative PLS weights for the curious reader).

Spatial permutation test (spin test): We assessed the significance of correlation between the neuroimaging biomarker and the selected PLS component using spatial permutation testing (spin test) to account for the inherent spatial autocorrelation of the imaging data, as implemented in previous studies[53-55]. This approach consists in comparing the empirical correlation amongst two spatial maps to a set of null correlations, generated by randomly rotating the spherical projection of one of the two spatial maps before projecting it back onto the brain parcel. Importantly, the rotated projection preserves the spatial contiguity of the empirical maps, as well as the hemispheric symmetry. Past studies using the spin test have focused on comparisons between brain maps including only cortical regions. However, subcortical regions were also of interest in this study. Since subcortical regions cannot be projected onto the inflated spherical pial surface, we incorporated the subcortex into our null models by shuffling the seven subcortical regions with respect to one another, whereas the cortical regions were shuffled using the spin test.

Gene set enrichment analyses. We used each neuroimaging biomarker-associated ordered list of genes, ranked by the respective weights according to the PLS component under investigation, to perform gene set enrichment analyses (GSEA) for biological pathways (gene ontology) and genes expressed in different brain cell types, as identified in previous single-cell transcriptomic studies (see section on single-cell transcriptomic data below). We implemented these analyses using the GSEA method of interest of the Web-based gene set analysis toolkit (*WebGestalt*)[56]. In contrast

to other over-representation methods, GSEA does not require the definition of an arbitrary threshold to isolate the most highly associated genes with a certain phenotype. It calculates an enrichment ratio (ER) that represents the degree to which the genes in the set are over-represented at either the top (positive ER) or bottom (negative ER) of the list, based on a Kolmogorov-Smirnov-like statistic. Then, it estimates the statistical significance of the ER using permutations to produce a null distribution for the ER (we used 1,000 permutations). The significance is determined by comparison to the null distribution. Finally, it adjusts for multiple hypothesis testing when several gene sets are being analysed at one time. The enrichment scores for each set are normalized (NER) to account for the number of genes in each gene set and a false discovery rate correction is applied.

Single-cell transcriptomic data. To define the transcriptomic profile of the brain cell types mentioned above, we relied on the single-cell transcriptomic data from the previous single-cell transcriptomic study of Lake et al. [57]. In this study, the authors used snDrop-seq Unique Molecular Identifier counts for cells from the visual (BA17) and dorsal frontal cortex (BA 6/9/10) and identified 30 brain cell-types (astrocytes, endothelial cells, pericytes, microglia, oligodendrocytes, oligodendrocytes progenitor cells (OPCs), 13 subtypes of excitatory neurons and 11 subtypes of inhibitory neurons). We decided to consider these 30 cells, since this classification provides a good coverage of a wide range of different neuronal and non-neuronal cells.

Sensitivity analyses. We assessed the robustness of our findings by performing a sensitivity analysis examining the impact of: i) brain parcellation; ii) transcriptomic profile of brain cell-types; and iii) inclusion of subcortical + cortical vs cortical regions only, when a whole brain receptor neuroimaging marker (e.g. [^{18}F]Fallypride) has higher binding in subcortical than cortical regions. These analyses are described in detail in Supplementary.

Data availability: While some of these templates are publicly available, others have been kindly shared by individual research groups. Access to these data might be granted upon to reasonable request by contacting directly principal investigators (see Appendix with all contributors and associated data).

Code availability: The code for performing the imaging transcriptomic analyses is now available as a python package that can be downloaded from https://github.com/molecular-neuroimaging/Imaging_Transcriptomics.

Results

We provide a summary of the pairwise correlations between all maps in Supplementary Figure S1. Of note, we found large correlations between the regional distribution of [^{11}C]BU99008 and L-[^{11}C]deprenyl-D2 (r=0.90, p_{spin} <0.001), and between [^{11}C]PBR28 and [^{11}C]ER176 (r=0.99, p_{spin} <0.001). Below, we present the results of the imaging transcriptomics analyses for each map, organized in three main subsections: i) neuroreceptors, synaptic proteins and metabolism; ii) astroglia and myelin; iii) 18-kDa Translocator protein (TSPO) and Cox-1.

Neuroreceptors, synaptic proteins and metabolism

[^{11}C]Flumazenil: The first PLS component explained the largest amount of variance (44.99%) and correlated positively with the regional distribution of [^{11}C]Flumazenil (r=0.6708, p_{spin} < 0.001) (Figure 2). We found enrichment among the most positively weighted genes for several gene ontology – biological process domain terms globally related to synaptic structure and transmission, including the glutamate receptor signalling pathway (NER=2.26, p_{FDR} = 0.001) and GABAergic synaptic transmission (NER=1.809, p_{FDR} = 0.02) (Supplementary data S2). The cell-type enrichment analysis indicated significant enrichment for several subclusters of excitatory and inhibitory neurons, with Ex6b emerging as the strongest enrichment hit. In addition to these neuronal subclusters, we also found significant enrichment for genes expressed in astrocytes and OPCs.

[^{18}F]GE179: The first PLS component explained the largest amount of variance (30.29%) and correlated positively with the regional distribution of [^{18}F]GE179 (r=0.5504, p_{spin} = 0.002) (Figure 2). We found enrichment among the most positively weighted genes for two gene ontology – biological process terms, namely the synapse organization (NER=2.07, p_{FDR} = 0.02) and GABA signalling pathway (NER=2.02, p_{FDR} = 0.02) (Supplementary data S2). The cell-type enrichment analysis indicated significant enrichment for several subclusters of excitatory and inhibitory neurons, with Ex8 emerging as the strongest enrichment hit.

[^{11}C]UCB-J: The first PLS component explained the largest amount of variance (30.92%) and correlated positively with the regional distribution of [^{11}C]UCB-J (r=0.5561, p_{spin} = 0.002) (Figure 2). We found enrichment among the most positively weighted genes for several gene ontology – biological process terms, including the neuropeptide signalling pathway (NER=2.11, p_{FDR} = 0.007), regulation of synaptic structure and activity (NER=1.98, p_{FDR} = 0.02) and glutamatergic synaptic transmission (NER=1.98, p_{FDR} = 0.02) (Supplementary data S2). The cell-type enrichment analysis indicated significant enrichment for several subclusters of excitatory and inhibitory neurons, with Ex6b emerging as the strongest enrichment hit.

[^{18}F]FDG: The first PLS component explained the largest amount of variance (42.28%) and correlated positively with the regional distribution of [^{18}F]FDG (r=0.6503, p_{spin} < 0.001) (Figure 2). We found enrichment among the most positively weighted genes for two gene ontology – biological process terms, which were peptide catabolic process (NER=1.97, p_{FDR} = 0.004) and protein dealkylation (NER=1.81, p_{FDR} = 0.007) (Supplementary data S2). The cell-type enrichment analysis indicated significant enrichment for several subclusters of excitatory and inhibitory neurons, with Ex3d emerging as the strongest enrichment hit. Among the non-neuronal cells, we also found enrichment for genes expressed in endothelial cells.

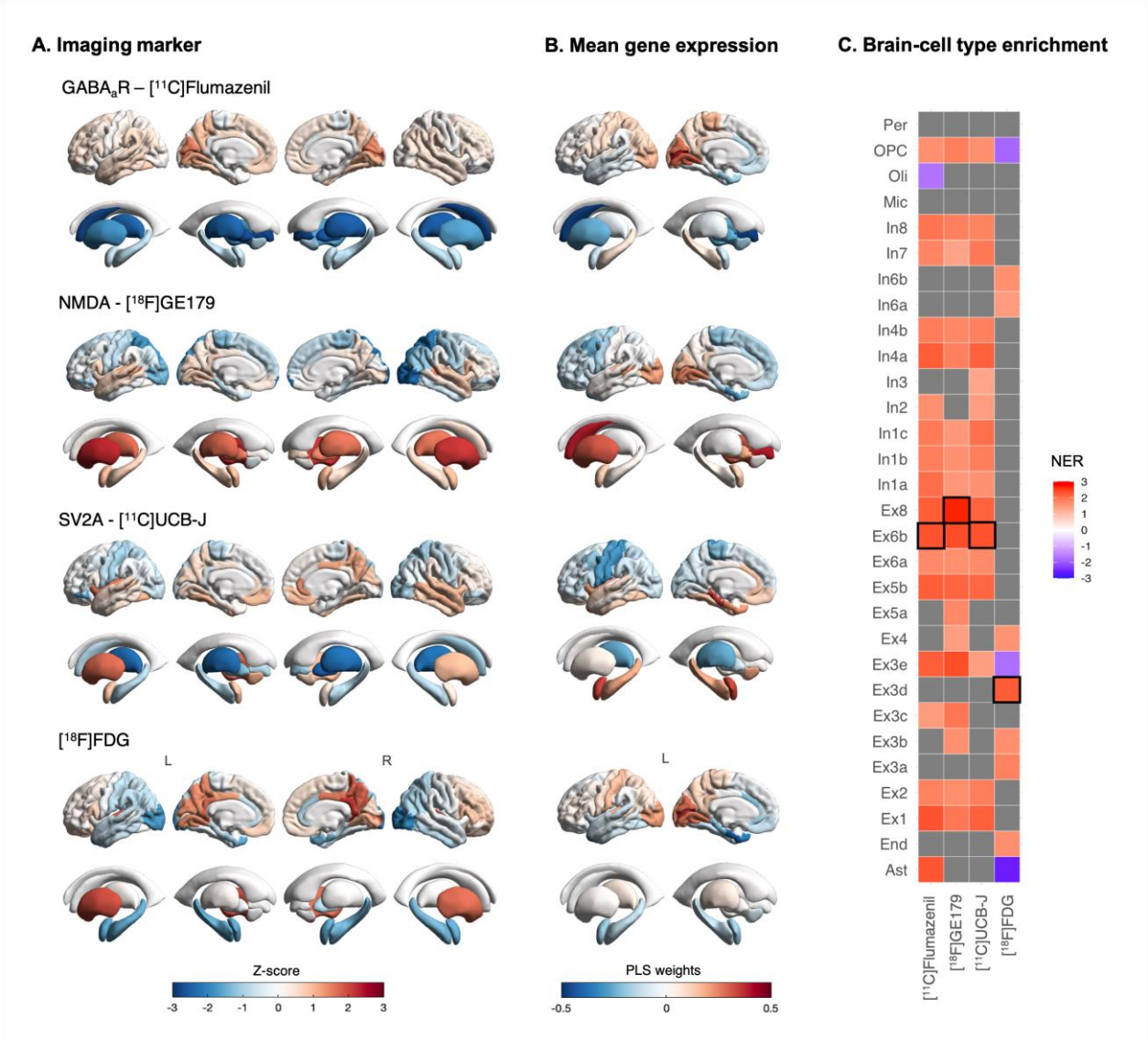

Figure 2. Imaging transcriptomics (neuroreceptors, synaptic proteins and metabolism). (A) - Regional distribution of each marker. (B) – Regional distribution of the PLS1 weights. (C) – Brain cell-type enrichment analyses: Positive normalized enrichment ratios (NER) indicate enrichment for genes of a certain brain cell-type among the genes with positive weights in PLS1 (i.e. positively correlated with the distribution of the neuroimaging marker); negative NERs indicate the reverse; grey squares indicate that the NER did not reach significance ($p_{FDR}>0.05$). The full statistics underlying the tile plot can be found in Supplementary data S1. Abbreviations: Ast – astrocytes; End – endothelial; Ex – excitatory neurons; In - inhibitory neurons; Mic – microglia; Oli – oligodendrocytes; OPC – oligodendrocyte precursor cells; Per – pericytes.

Astroglia and myelin

[^{11}C]BU99008: The first PLS component explained the largest amount of variance (42.01%) and correlated positively with the regional distribution of [^{11}C]BU99008 (r=0.6482, $p_{spin} < 0.001$) (Figure 3). We found enrichment among the most positively weighted genes for several gene ontology – biological process terms,

globally related to protein targeting, RNA and ribonucleoproteins metabolism, and the GABA signalling pathway (Supplementary data S2). The cell-type enrichment analysis indicated significant enrichment for some subclusters of inhibitory neurons and one subcluster of excitatory neurons. Astrocytes emerged as the strongest enrichment hit. In addition, we also found significant enrichment for genes expressed in OPCs and Pericytes.

L-[^{11}C]deprenyl-D2: The first PLS component explained the largest amount of variance (41.47%) and correlated positively with the regional distribution of L-[^{11}C]deprenyl-D2 ($r=0.6440$, $p_{spin} < 0.001$) (Figure 3). We found enrichment among the most positively weighted genes for several gene ontology – biological process terms, globally related to protein targeting, RNA and ribonucleoproteins metabolism (Supplementary data S2). The cell-type enrichment analysis indicated significant enrichment for some subclusters of inhibitory neurons and one subcluster of excitatory neurons. Astrocytes emerged as the strongest enrichment hit. In addition, we also found significant enrichment for genes expressed in OPCs.

Magnetization transfer ratio (MT): The first PLS component explained the largest amount of variance (34.91%) and correlated positively with the regional distribution of MT ($r=0.5909$, $p_{spin} < 0.001$) (Figure 3). We found enrichment among the most positively weighted genes for several gene ontology – biological process terms, globally related to extracellular structure organization, endothelium development and immune response (Supplementary data S2). The cell-type enrichment analysis indicated significant enrichment for all non-neuronal cells. Oligodendrocytes emerged as the strongest enrichment hit.

Myelin water content (WC): The first PLS component explained the largest amount of variance (31.40%) and correlated positively with the regional distribution of MT ($r=0.5604$, $p_{spin} = 0.007$) (Figure 3). We found enrichment among the most positively weighted genes for several gene ontology – biological process terms, globally related to amino acid biosynthetic processes, extracellular structure organization, endothelium development and angiogenesis, cell adhesion mediated by integrins and immune response (Supplementary data S2). The cell-type enrichment analysis indicated significant enrichment for all non-neuronal cells. Oligodendrocytes emerged as the strongest enrichment hit.

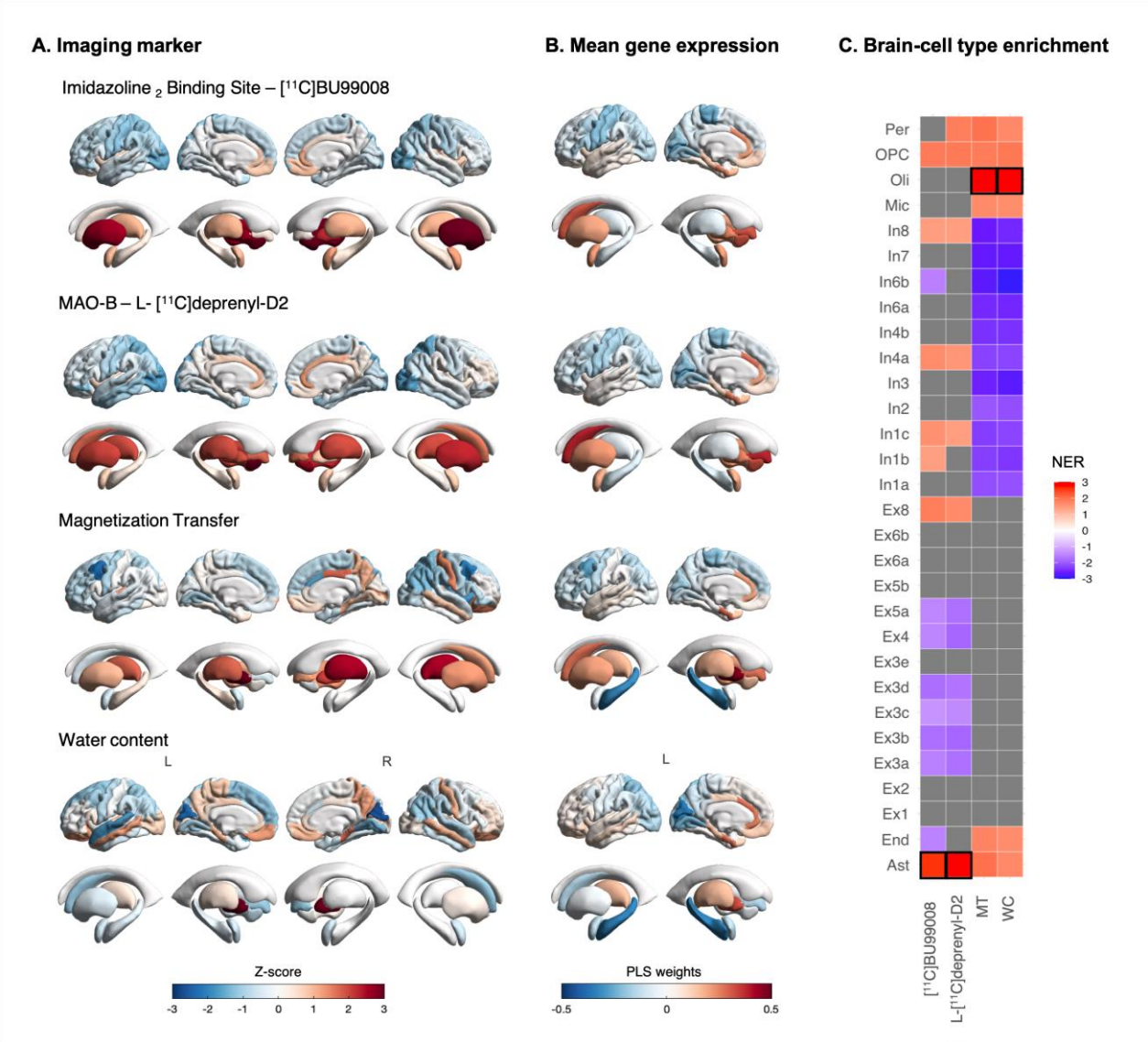

Figure 3. Imaging transcriptomics (astroglia and myelin). (A) - Regional distribution of each marker. (B) – Regional distribution of the PLS1 weights. (C) – Brain cell-type enrichment analyses: Positive normalized enrichment ratios (NER) indicate enrichment for genes of a certain brain cell-type among the genes with positive weights in PLS1 (i.e., positively correlated with the distribution of the neuroimaging marker); negative NERs indicate the reverse; grey squares indicate that the NER did not reach significance ($p_{FDR}>0.05$); The full statistics underlying the tile plot can be found in Supplementary data S1. Abbreviations: Ast – astrocytes; End – endothelial; Ex – excitatory neurons; In - inhibitory neurons; Mic – microglia; Oli – oligodendrocytes; OPC – oligodendrocyte precursor cells; Per – pericytes.

18-kDa translocator protein (TSPO) and cyclooxygenase (Cox)

TSPO - [^{11}C]PK11195: The first PLS component explained the largest amount of variance (36.30%) and correlated positively with the regional distribution of [^{11}C]PK11195 ($r=0.6025$, $p_{spin} < 0.001$) (Figure 4). We found enrichment among the most positively weighted genes for several gene ontology – biological process terms,

including metabolic processes, granulocyte activation and response to interferon gamma, ensheathment of neurons, and DNA repair (Supplementary data S2). The cell-type enrichment analysis indicated significant enrichment for all non-neuronal cells, excluding astrocytes. Microglia emerged as the strongest enrichment hit.

TSPO - [^{18}F]DPA174: The first PLS component explained the largest amount of variance (33.23%) and correlated positively with the regional distribution of [^{18}F]DPA174 (r=0.5765, p_{spin} = 0.001) (Figure 4). We did not find enrichment among the most positively weighted genes for any of the gene ontology – biological process terms. The cell-type enrichment analysis indicated significant enrichment for all non-neuronal cells, excluding astrocytes and oligodendrocytes. In contrast with [^{11}C]PK11195, here we also found enrichment for several subclusters of excitatory and inhibitory cells. Pericytes emerged as the strongest enrichment hit.

TSPO - [^{18}C]PBR28: The first PLS component explained the largest amount of variance (34.66%) and correlated positively with the regional distribution of [^{18}C]PBR28 (r=0.5887, p_{spin} = 0.001) (Figure 4). We did not find enrichment among the most positively weighted genes for any of the gene ontology – biological process terms. The cell-type enrichment analysis indicated significant enrichment for pericytes, oligodendrocytes, endothelial cells and several subclusters of excitatory and inhibitory cells. Endothelial cells emerged as the strongest enrichment hit.

TSPO - [^{18}C]ER176: The first PLS component explained the largest amount of variance (36.60%) and correlated positively with the regional distribution of [^{18}C]ER176 (r=0.6050, p_{spin} < 0.001) (Figure 4). We did not find enrichment among the most positively weighted genes for any of the gene ontology – biological process terms. The cell-type enrichment analysis indicated significant enrichment for pericytes, oligodendrocytes, endothelial cells and several subclusters of excitatory and inhibitory cells. Endothelial cells emerged as the strongest enrichment hit.

COX-1 - [^{11}C]PS13: The first PLS component explained the largest amount of variance (41.22%) and correlated positively with the regional distribution of [^{11}C]PS13 (r=0.6420, p_{spin} < 0.001) (Figure 4). We did not find enrichment among the most positively weighted genes for any of the gene ontology – biological process terms. The cell-type enrichment analysis indicated significant enrichment for pericytes, microglia, endothelial cells and several subclusters of excitatory and inhibitory cells, with Ex3d emerging as the strongest enrichment hit

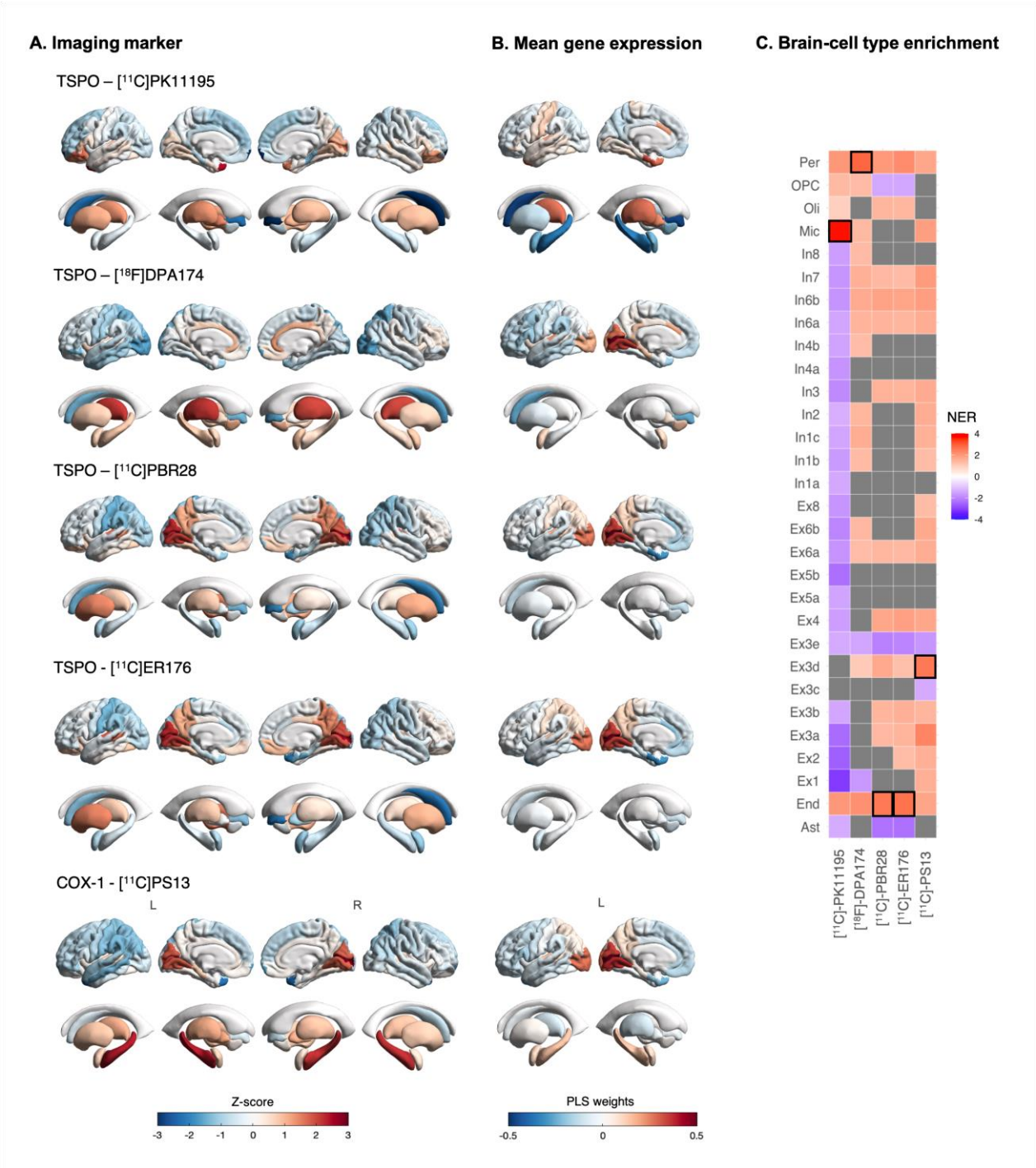

Figure 4. Imaging transcriptomics (Translocator protein and cyclooxygenase). (A) - Regional distribution of each marker. (B) – Regional distribution of the PLS1 weights. (C) – Brain cell-type enrichment analyses: Positive normalized enrichment ratios (NER) indicate enrichment for genes of a certain brain cell-type among the genes with positive weights in PLS1 (i.e. positively correlated with the distribution of the neuroimaging marker); negative NERs indicate the reverse; grey squares indicate that the NER did not reach significance (p_{FDR}>0.05); The full statistics underlying the tile plot can be found in Supplementary data S1. Abbreviations: Ast – astrocytes; End – endothelial; Ex – excitatory neurons; In - inhibitory neurons; Mic – microglia; Oli – oligodendrocytes; OPC – oligodendrocyte precursor cells; Per – pericytes.

Sensitivity analyses:

Brain parcellation. We found large correlations (Pearson's r between 0.79 and 0.94) between PLS1 weights of all genes as estimated using the DK and AAL3 atlases (Supplementary Table S1).

Brain cell-types transcriptomic profile. Changing the gene sets used to define the transcriptomic profile of each brain cell-type did not considerably change our main brain cell-type enrichment conclusions (Supplementary data S3).

Inclusion of cortical + subcortical regions vs cortical regions only. By including both cortical and subcortical regions in the same model, we identified the DRD2 gene as one of the top genes positively associated with [^{18}F]fallypride binding (Z = 5.17, Rank: 161/15,633, top 1% of all genes). When repeating the same analysis with cortical regions, we still identified *DRD2* as a positively weighted gene, but its rank was considerably lower (Z = 3.67, Rank: 2,204/15,633, top 15% of all genes) (Supplementary Figure S2).

Discussion

In this work, we investigated whether imaging transcriptomics can recover plausible transcriptomic and cellular correlates of the regional distribution of benchmark molecular imaging markers. With the recent upsurge of imaging transcriptomics studies, this work is crucial to strengthening our confidence in the plausibility of this integrative approach as an indirect way to generate hypotheses about potential biological pathways explaining regional variations in *in vivo* neuroimaging biomarkers. This is of particular importance for those neuroimaging markers where more fine-grained biological mechanisms cannot be measured directly. Thanks to an unprecedented collaborative effort, we gathered a vast number of tracers spanning different elements of the brain's biology, which allowed us to conduct a comprehensive evaluation of the plausibility of the approach across different biological and cellular pathways. In a set of secondary analyses, we confirmed that the method is likely to generalize well beyond the specific choices of brain parcellation or gene sets used to define the transcriptomic profile of brain cell-types. Altogether, our data supports the plausibility and robustness of imaging transcriptomics as an indirect approach bridging levels between gene expression, cells and macroscopical neuroimaging to improve our understanding of the biological pathways underlying regional variability in neuroimaging features.

Our first set of analyses were focused on four markers targeting neuroreceptors (GABA-A and NMDA receptors), a synaptic protein (SV2A) and metabolism (FDG). We hypothesized that the regional distribution of these markers would align preferentially with the distribution of genes involved in synaptic structure and neurotransmission, which are highly expressed in populations of neuronal cells. In line with our main hypotheses, this was what we found. The $GABA_A$ receptor is the major target for GABA, an inhibitory neurotransmitter found in about 20–50% of synapses in the brain [58]. This receptor is predominantly located in the postsynaptic membrane and can be expressed by both excitatory and inhibitory neurons[59]; however, it also localizes at extra-synaptic sites. For instance, it has become increasingly clear that astrocytes, both in cell culture and in tissue slices, express abundant $GABA_A$ receptors [60]. This aspect might explain why, in addition to neuronal cells, we also found enrichment for astrocytic genes among the top genes positively associated with [^{11}C]Flumazenil binding.

The NMDA receptor is a glutamate receptor predominantly located in the post-synaptic membrane of neurons, which participates in neuronal excitation and plasticity[61-63]. It is present at both excitatory and inhibitory neurons [64,65]; but there are also reports of its expression in oligodendrocytes and OPCs[66,67]. While we found enrichment among the genes positively associated with NMDA regional distribution for several clusters of excitatory and inhibitory neurons and oligodendrocytes progenitors, we did not find enrichment for genes highly expressed in mature oligodendrocytes. This could reflect the fact that expression of NMDA receptors in oligodendrocytes is only minoritarian as compared to neurons, which might be insufficient to generate a pattern of distribution that would strongly align with oligodendrocyte genes.

The synaptic vesicle glycoprotein 2A (SV2A) is a prototype presynaptic vesicle protein regulating action potential-dependent neurotransmitters release, which is expressed across both excitatory and inhibitory neurons [68,69]. This cellular distribution aligns well with the fact that we found enrichment among the genes positively associated with SV2A regional distribution for several clusters of excitatory and inhibitory neurons. To our knowledge, there have not been reports of high constitutive expression of SV2A in OPCs even if we found enrichment for genes highly

expressed in these cells; however, since OPCs can also differentiate into neurons[70], it is not implausible that SV2A might also be present in OPCs and colocalize with other elements of the molecular machinery of these cells.

[^{18}F]FDG is a metabolic marker typically used as a fully quantitative indirect index of neuronal activity as it captures the cerebral glucose uptake[71,72]. A long-standing model postulates that the use of glucose by neurons requires an interplay with astrocytes in an astrocyte-to-neuron lactate shuttle mechanism, where glucose is taken up by astrocytes and converted to lactate, which is then oxidized by neurons[73]. In line with this model, the contribution of astrocytes to [^{18}F]FDG signal has recently been elegantly demonstrated in the rodent brain after activation of astrocytic glutamate transport[74]. However, this model has been debated over the last decade after some animal evidence has shown that: i) glucose is taken up preferentially by neurons in awake behaving mice; ii) hexokinase, which catalyses the first enzymatic steps in glycolysis, is highly enriched in neurons as compared to astrocytes, in both mouse and human cortex[75]. Our brain cell-type enrichment analysis is consistent with this last model of glucose uptake by neurons by showing predominance of genes highly expressed in neurons. Interestingly, we also found enrichment for genes highly expressed in endothelial cells, which are known to uptake [^{18}F]FDG using similar mechanisms to those used by neurons[76]. However, astrocytic genes were mostly anti-correlated with [^{18}F]FDG (i.e. enrichment of astrocyte genes among genes negatively weighted). Whether this simply reflects species differences or the fact that our [^{18}F]FDG scans were acquired at rest (while in the abovementioned rodent study[74], [^{18}F]FDG signal was measured in response to astrocytic glutamate transport) deserves further exploration. Altogether, these data support the plausibility of imaging transcriptomics in capturing patterns of constitutive gene expression that align well with different elements of the neuronal biology.

Our second set of analyses was focused on two tracers typically used as astrocyte probes and two MRI maps sensitive to myelin. Here, our findings broadly supported our hypothesis that by using imaging transcriptomics we would be able to identify patterns of gene expression consistent with astrocyte and oligodendrocyte genes, respectively. For both [^{11}C]BU99008 and L-[^{11}C]deprenyl-D2 we did find enrichment among the top genes positively associated with the regional distribution of these tracers for genes highly expressed in astrocytes and belonging to biological processes that are relevant to astrocytic biology, such as protein targeting (which is a key regulator of glycogen synthesis in astrocytes[77]) and RNA and ribonucleoproteins metabolism (which participate in local translation of transcripts in astrocytic peripheral processes[78]). In addition to astrocytes, we also found enrichment for genes highly expressed in some subclusters of neurons. This is not entirely surprising for the following reasons. [^{11}C]BU99008 binds the imidazoline$_2$ binding site (I_2BS), which is thought to be expressed in glia and implicated in the regulation of glial fibrillary acidic protein[79,80]. Despite the lack of consensus regarding the nature of I_2 receptors, cellular distribution studies revealed that I_2BS are primarily located on the outer membrane of mitochondria and may be novel allosteric binding sites of monoamine oxidases (MAO) A and B[81-83]. Few studies have addressed the issue of which cell types in brain (neurones and/or glia) express I_2BS. However, few different studies seem to agree that I_2BS is expressed in both neurons and astroglia[84]. Similarly, L-[^{11}C]deprenyl-D2 is a radiotracer which binds to MAO-B[85]. MAO-B is found in the brain primarily in non-neuronal cells such as astrocytes and radial glia, but immunohistochemistry studies have also reported the presence of MAO-B in neurons[86-88].

For both MT ratio and myelin WC, we found enrichment for genes highly expressed in oligodendrocytes and OPCs, which matches the know sensitivity of these MRI markers to myelin[89,90]. However, we also found enrichment for other non-neuronal cells, such as microglia, astrocytes, pericytes and endothelial cells. This observation is intriguing and dovetails with recent controversies about the interpretation of MT and WC as specific markers for myelin, particularly in the grey matter[91-94]. For instance, the MT phenomena can occur in any large macromolecule with low molecular tumbling rate, making the measure sensitive to a variety of cellular processes (such as dendrites or myelin), but specific to virtually none[95]. Altogether, these data support the plausibility of imaging transcriptomics in capturing patterns of constitutive gene expression that align well with different elements of the astroglia and oligodendrocytes biology.

Our third set of analyses was conducted on four TSPO tracers and one tracer for Cox-1, which we hypothesized to be in line with the regional constitutive expression of genes involved in the neuroimmune response axis, such as those expressed in microglia or astrocytes. TSPO is expressed ubiquitously in the body and is used as a biomarker of neuroinflammation because its upregulation in inflammatory conditions is strongly localized to microglia and macrophages. Cyclooxygenase (COX) enzymes perform the rate-limiting step in the synthesis of inflammatory mediators such as prostaglandins and thromboxanes from arachidonic acid. The two main isoforms, COX-1 and COX-2 are present constitutively in the brain. COX-1 is predominantly localized in microglia in the brain. In contrast to our predictions, apart from [^{11}C]PK11195, microglia and astrocyte genes were not among the top enrichment hits for all the other TSPO and Cox-1 tracers. Instead, for [^{18}F]DPA174, the top enrichment hit was pericytes, but we also found enrichment for microglia genes; for [^{18}C]PBR28 and [^{18}C]ER176, the top enrichment hit was endothelial cells, but enrichment for microglia genes was not present. For [^{11}C]PS13, the top enrichment hit was the excitatory neurons subcluster 3d, but enrichment for microglia was also present.

At first, these results might seem contradictory, but they need to be considered within the context of our recent increasing understanding of the biology of TSPO[96] and methodological challenges that pervade in-vivo TSPO quantification in the human brain[97]. TSPO is an evolutionarily conserved protein localized in the outer mitochondrial membrane, which has been linked to various (but not mutually exclusive) physiological processes, such as cholesterol transport and steroid hormone synthesis, apoptosis and cell viability, redox processes and oxidative stress, and mitochondrial respiration and bioenergetics[96,98]. Recent evidence suggests that TSPO expression is spread across several brain cell-types and single cell quantifications of its constitutive expression suggest that basal TSPO mRNA expression is most abundant in ependymal cells, vascular endothelial cells, and microglia[99]; its expression is also detectable in neurons, even though in very low quantities and possibly modulated by neuronal activity[99]. Therefore, our findings for the TSPO tracers, namely a consistent enrichment for pericytes and endothelial cells, are broadly in line with this recent view of the cell-type relative expression distribution of TSPO. Only for [^{11}C]PK11195, which is a first-generation tracer associated with low amounts of specific binding[97], we identified microglia as the strongest enrichment hit; in contrast, for the other three second-generation tracers, which have demonstrated superior specificity [97], we did not. We also noted that while the TSPO gene was among the genes most positively correlated with the distribution of [^{11}C]PK11195 (Z=3.08, Rank = 932/15,633), all the other three tracers were mostly unrelated to the distribution of TSPO mRNA ([^{18}F]DPA174: Z=0.40, Rank=6866/15,633; [^{18}C]PBR28: Z=-2.18, Rank=13,533/15,633;

[^{18}C]ER176: Z=-2.38, Rank=13,612/15,633). These findings are puzzling; however, admittedly, direct comparisons between tracers in this study are rather complex because of the use of different methods of quantification for the different tracers[97], different imaging facilities and different subjects. In this work, we used templates where quantification was implemented as per the original respective publications, accounting for the different subject TSPO genetic polymorphisms by excluding low-affinity binders[100]. Here, we did not intend to identify which of these four tracers might perform better in capturing TSPO or examine the impact of the quantification approach in the correlations of different tracers with TSPO mRNA. We strongly believe such endeavour deserves its own comprehensive evaluation (for a thorough review about the complexity around TSPO quantification see Turkheimer et al.[101]). Instead, we examined different tracers to triangulate findings, which altogether dovetail with the known complexity of TSPO biology and quantification[96,97]. For Cox-1, the strongest enrichment hit was one subcluster of excitatory neurons, but as predicted we also found enrichment for microglia. This observation matches previous reports describing expression of Cox-1 in both neurons and microglia, but not astrocytes[102]. Moreover, we also note the enrichment for endothelial cells and pericytes, which aligns with descriptions of expression of Cox-1 in endothelial cells and its role in regulating the synthesis of prostacyclins in the cerebrovasculature[103,104].

Our findings should be interpreted within the context of some limitations. First, given that most PET tracers do not have affinity for a single cell-type, our data should not be taken as an absolute validation of the imaging transcriptomics approach, since most likely tracer binding reflects contributions from more than one cell type. Instead, here, we examined whether the results of our enrichment analyses were plausible, given the known molecular nature of the tracers. Currently, we do not have access to dense phenotyping of the distribution of different brain cell types across the whole human brain, which admittedly would have been our first option for this work if existent. In the absence of this knowledge, PET provides only a practical approximation. Second, while still a general limitation of the field and not of this specific work, the AHBA whole-brain gene expression data derives only from six *post-mortem* adult brains (mean age = 43 y) and includes data in the right hemisphere from two donors, which led us to exclude the right hemisphere for the transcriptomic association analyses. Third, here we focused on comparisons between neuroimaging markers in the healthy adult human brain and constitutive gene expression in the healthy post-mortem brain. This does not detract that the strongest source of tracer binding might follow other biological pathways in pathology. A simple example is TSPO, which might be upregulated in microglia and astrocytes during neuroinflammation; in that case, if the disease process recruits the neuroimmune axis globally, then it is more likely that the TSPO distribution might better follow the constitutive regional distribution of astrocytes/microglia genes; while in the healthy brain, the signal might mirror better the endothelial component. In a similar way the radiotracer non displaceable non-specific binding might lead to spurious correlations. A simple example of this is represented by [^{18}F]GE179, which has shown to suffer from low specific binding when used at baseline[105]. Fourth, by using constitutive gene expression in a small cohort of six post-mortem brains to infer associations with neuroimaging markers acquired in different cohorts, we are assuming that regional gene expression is a conserved canonical signature that generalizes well beyond the brain samples included in the AHBA. While we focused our analyses on probes that were selected to maximize differential stability across donors, six post-mortem brains are insufficient to make strong claims about the stability of gene expression across brains in humans. This might be a bigger concern for mobile brain

cells that can dynamically move within the brain parenchyma, such as microglia, which participate in immunosurveillance even at rest[106]; this mobility might – at least theoretically – result in higher variability in gene expression across individuals and deserves further exploration. Fifth, no replicability analyses on independent datasets (same tracer, same experimental protocol and analysis, but different subjects) were performed. To our knowledge this work has been able to pull together an unprecedent number and varieties of brain scans. However, with the brain PET community recognising the importance of open data sharing (e.g. OpenNeuroPET, https//openneuro.org/pet)[107], such endeavour might be feasible in the near future. Finally, our findings do show robustness to the specific choice of parcellation and set of single-cell genes used in our main analyses. For instance, we found large correlations between PLS1 genes weights between the analyses performed with the DK and AAL3 atlases; we also found that changing the set of genes used to define brain cell-types did not change our main conclusions considerably. However, it also true that both imaging and mRNA findings can be quite dependent on the particular methodology used to analyse the data. More work would in this topic should follow to ensure reproducibility and replicability.

In summary, our data supports the value and robustness of integrative imaging transcriptomics analyses in recovering plausible transcriptomic and cellular correlates of the regional distribution of a range of benchmark molecular imaging markers spanning different elements of the biology of the brain. The application of this indirect approach to bridge levels between gene expression, cells and macroscopical neuroimaging phenotypes holds the potential to improve our understanding of the biological pathways underlying regional variability in neuroimaging features. As a result, imaging transcriptomics could open new opportunities to expand the outputs of the use of neuroimaging tools in clinical research by: i) refining models of brain disease with the inclusion of more mechanistic biological information; ii) advancing the understanding of the role that genetic factors might play in brain regional vulnerability in brain disease; and iii) helping prioritizing targets for drug development or development of preclinical models with high translational value.

List of Supplementary Materials:

Supplementary methods: PET templates (full description).

Supplementary methods: Sensitivity analyses

Supplementary Figure S1. Correlations between neuroimaging markers.

Supplementary Table S1. Sensitivity analysis – brain parcellation.

Supplementary Figure S2. Sensitivity analysis – cortical + subcortical regions vs cortical regions only.

References:

1 Brammer, M. The role of neuroimaging in diagnosis and personalized medicine--current position and likely future directions. *Dialogues Clin Neurosci* **11**, 389-396 (2009).

2 Writing Committee for the Attention-Deficit/Hyperactivity, D. *et al.* Virtual Histology of Cortical Thickness and Shared Neurobiology in 6 Psychiatric Disorders. *JAMA Psychiatry* **78**, 47-63, doi:10.1001/jamapsychiatry.2020.2694 (2021).

3 Opel, N. *et al.* Cross-Disorder Analysis of Brain Structural Abnormalities in Six Major Psychiatric Disorders: A Secondary Analysis of Mega- and Meta-analytical Findings From the ENIGMA Consortium. *Biol Psychiatry* **88**, 678-686, doi:10.1016/j.biopsych.2020.04.027 (2020).

4 Cassidy, P. J. & Radda, G. K. Molecular imaging perspectives. *J R Soc Interface* **2**, 133-144, doi:10.1098/rsif.2005.0040 (2005).

5 Shen, E. H., Overly, C. C. & Jones, A. R. The Allen Human Brain Atlas: comprehensive gene expression mapping of the human brain. *Trends Neurosci* **35**, 711-714, doi:10.1016/j.tins.2012.09.005 (2012).

6 Rizzo, G. *et al.* The predictive power of brain mRNA mappings for in vivo protein density: a positron emission tomography correlation study. *J Cereb Blood Flow Metab* **34**, 827-835, doi:10.1038/jcbfm.2014.21 (2014).

7 Arnatkeviciute, A., Fulcher, B. D. & Fornito, A. A practical guide to linking brain-wide gene expression and neuroimaging data. *Neuroimage* **189**, 353-367, doi:10.1016/j.neuroimage.2019.01.011 (2019).

8 Patel, Y. *et al.* Virtual histology of multi-modal magnetic resonance imaging of cerebral cortex in young men. *Neuroimage* **218**, 116968, doi:10.1016/j.neuroimage.2020.116968 (2020).

9 Patania, A. *et al.* Topological gene expression networks recapitulate brain anatomy and function. *Netw Neurosci* **3**, 744-762, doi:10.1162/netn_a_00094 (2019).

10 Romero-Garcia, R. *et al.* Structural covariance networks are coupled to expression of genes enriched in supragranular layers of the human cortex. *Neuroimage* **171**, 256-267, doi:10.1016/j.neuroimage.2017.12.060 (2018).

11 Shin, J. *et al.* Cell-Specific Gene-Expression Profiles and Cortical Thickness in the Human Brain. *Cereb Cortex* **28**, 3267-3277, doi:10.1093/cercor/bhx197 (2018).

12 Seidlitz, J. *et al.* Morphometric Similarity Networks Detect Microscale Cortical Organization and Predict Inter-Individual Cognitive Variation. *Neuron* **97**, 231-247 e237, doi:10.1016/j.neuron.2017.11.039 (2018).

13 Liu, S., Seidlitz, J., Blumenthal, J. D., Clasen, L. S. & Raznahan, A. Integrative structural, functional, and transcriptomic analyses of sex-biased brain organization in humans. *Proc Natl Acad Sci U S A* **117**, 18788-18798, doi:10.1073/pnas.1919091117 (2020).

14 Shen, J. *et al.* Cell-Type-Specific Gene Modules Related to the Regional Homogeneity of Spontaneous Brain Activity and Their Associations With Common Brain Disorders. *Front Neurosci* **15**, 639527, doi:10.3389/fnins.2021.639527 (2021).

15 Tang, J. *et al.* Brain Gene Expression Pattern Correlated with the Differential Brain Activation by Pain and Touch in Humans. *Cereb Cortex*, doi:10.1093/cercor/bhab028 (2021).

16 Zhu, D. *et al.* Correlation between cortical gene expression and resting-state functional network centrality in healthy young adults. *Hum Brain Mapp* **42**, 2236-2249, doi:10.1002/hbm.25362 (2021).

17 Hansen, J. Y. *et al.* Mapping gene transcription and neurocognition across human neocortex. *Nat Hum Behav*, doi:10.1038/s41562-021-01082-z (2021).

18 Wen, J., Goyal, M. S., Astafiev, S. V., Raichle, M. E. & Yablonskiy, D. A. Genetically defined cellular correlates of the baseline brain MRI signal. *Proc Natl Acad Sci U S A* **115**, E9727-E9736, doi:10.1073/pnas.1808121115 (2018).

19 Diez, I. & Sepulcre, J. Neurogenetic profiles delineate large-scale connectivity dynamics of the human brain. *Nat Commun* **9**, 3876, doi:10.1038/s41467-018-06346-3 (2018).

20 Richiardi, J. *et al.* BRAIN NETWORKS. Correlated gene expression supports synchronous activity in brain networks. *Science* **348**, 1241-1244, doi:10.1126/science.1255905 (2015).

21 Forsyth, J. *et al.* Prioritizing Genetic Contributors to Cortical Alterations in 22q11.2 Deletion Syndrome Using Imaging Transcriptomics. *Cereb Cortex*, doi:10.1093/cercor/bhab008 (2021).

22 Hess, J. L., Radonjic, N. V., Patak, J., Glatt, S. J. & Faraone, S. V. Autophagy, apoptosis, and neurodevelopmental genes might underlie selective brain region vulnerability in attention-deficit/hyperactivity disorder. *Mol Psychiatry*, doi:10.1038/s41380-020-00974-2 (2020).

23 Altmann, A. *et al.* Analysis of brain atrophy and local gene expression in genetic frontotemporal dementia. *Brain Commun* **2**, doi:10.1093/braincomms/fcaa122 (2020).

24 Ji, Y. *et al.* Genes associated with gray matter volume alterations in schizophrenia. *Neuroimage* **225**, 117526, doi:10.1016/j.neuroimage.2020.117526 (2021).

25 Anderson, K. M. *et al.* Convergent molecular, cellular, and cortical neuroimaging signatures of major depressive disorder. *Proc Natl Acad Sci U S A* **117**, 25138-25149, doi:10.1073/pnas.2008004117 (2020).

26 Keo, A. *et al.* Transcriptomic signatures of brain regional vulnerability to Parkinson's disease. *Commun Biol* **3**, 101, doi:10.1038/s42003-020-0804-9 (2020).

27 Romero-Garcia, R. *et al.* Schizotypy-Related Magnetization of Cortex in Healthy Adolescence Is Colocated With Expression of Schizophrenia-Related Genes. *Biol Psychiatry* **88**, 248-259, doi:10.1016/j.biopsych.2019.12.005 (2020).

28 Morgan, S. E. *et al.* Cortical patterning of abnormal morphometric similarity in psychosis is associated with brain expression of schizophrenia-related genes. *Proc Natl Acad Sci U S A* **116**, 9604-9609, doi:10.1073/pnas.1820754116 (2019).

29 Li, J. *et al.* Cortical structural differences in major depressive disorder correlate with cell type-specific transcriptional signatures. *Nat Commun* **12**, 1647, doi:10.1038/s41467-021-21943-5 (2021).

30 Jimenez-Marin, A. *et al.* Transcriptional Signatures of Synaptic Vesicle Genes Define Myotonic Dystrophy Type I Neurodegeneration. *Neuropathol Appl Neurobiol*, doi:10.1111/nan.12725 (2021).

31 Seidlitz, J. *et al.* Transcriptomic and cellular decoding of regional brain vulnerability to neurogenetic disorders. *Nat Commun* **11**, 3358, doi:10.1038/s41467-020-17051-5 (2020).

32 Parker, N. *et al.* Assessment of Neurobiological Mechanisms of Cortical Thinning During Childhood and Adolescence and Their Implications for Psychiatric Disorders. *JAMA Psychiatry* **77**, 1127-1136, doi:10.1001/jamapsychiatry.2020.1495 (2020).

33 Vasa, F. *et al.* Conservative and disruptive modes of adolescent change in human brain functional connectivity. *Proc Natl Acad Sci U S A* **117**, 3248-3253, doi:10.1073/pnas.1906144117 (2020).

34 Fenchel, D. *et al.* Development of Microstructural and Morphological Cortical Profiles in the Neonatal Brain. *Cereb Cortex* **30**, 5767-5779, doi:10.1093/cercor/bhaa150 (2020).

35 Rizzo, G., Veronese, M., Expert, P., Turkheimer, F. E. & Bertoldo, A. MENGA: A New Comprehensive Tool for the Integration of Neuroimaging Data and the Allen Human Brain Transcriptome Atlas. *PLoS One* **11**, e0148744, doi:10.1371/journal.pone.0148744 (2016).

36 Selvaggi, P., Rizzo, G., Mehta, M. A., Turkheimer, F. E. & Veronese, M. Integration of human whole-brain transcriptome and neuroimaging data: Practical considerations of current available methods. *J Neurosci Methods* **355**, 109128, doi:10.1016/j.jneumeth.2021.109128 (2021).

37 Gryglewski, G. *et al.* Spatial analysis and high resolution mapping of the human whole-brain transcriptome for integrative analysis in neuroimaging. *Neuroimage* **176**, 259-267, doi:10.1016/j.neuroimage.2018.04.068 (2018).

38 Hammers, A. *et al.* [11C]Flumazenil PET in temporal lobe epilepsy: do we need an arterial input function or kinetic modeling? *J Cereb Blood Flow Metab* **28**, 207-216, doi:10.1038/sj.jcbfm.9600515 (2008).

39 McGinnity, C. J. *et al.* Initial evaluation of 18F-GE-179, a putative PET Tracer for activated N-methyl D-aspartate receptors. *J Nucl Med* **55**, 423-430, doi:10.2967/jnumed.113.130641 (2014).

40 Tyacke, R. J. *et al.* Evaluation of (11)C-BU99008, a PET Ligand for the Imidazoline2 Binding Site in Human Brain. *J Nucl Med* **59**, 1597-1602, doi:10.2967/jnumed.118.208009 (2018).

41 Albrecht, D. S. *et al.* Brain glial activation in fibromyalgia - A multi-site positron emission tomography investigation. *Brain, behavior, and immunity* **75**, 72-83, doi:10.1016/j.bbi.2018.09.018 (2019).

42 Schubert, J. J. *et al.* A Modest Increase in (11)C-PK11195-Positron Emission Tomography TSPO Binding in Depression Is Not Associated With Serum C-Reactive Protein or Body Mass Index. *Biol Psychiatry Cogn Neurosci Neuroimaging*, doi:10.1016/j.bpsc.2020.12.017 (2021).

43 Veronese, M. *et al.* Parametric Mapping for TSPO PET Imaging with Spectral Analysis Impulsive Response Function. *Mol Imaging Biol*, doi:10.1007/s11307-020-01575-9 (2021).

44 Zanotti-Fregonara, P. *et al.* Head-to-head comparison of (11)C-PBR28 and (11)C-ER176 for quantification of the translocator protein in the human brain. *Eur J Nucl Med Mol Imaging* **46**, 1822-1829, doi:10.1007/s00259-019-04349-w (2019).

45 Kim, M. J. *et al.* First-in-human evaluation of [(11)C]PS13, a novel PET radioligand, to quantify cyclooxygenase-1 in the brain. *Eur J Nucl Med Mol Imaging* **47**, 3143-3151, doi:10.1007/s00259-020-04855-2 (2020).

46 O'Muircheartaigh, J. *et al.* Quantitative neuroimaging measures of myelin in the healthy brain and in multiple sclerosis. *Hum Brain Mapp* **40**, 2104-2116, doi:10.1002/hbm.24510 (2019).

47 Neeb, H., Schenk, J. & Weber, B. Multicentre absolute myelin water content mapping: Development of a whole brain atlas and application to low-grade multiple sclerosis. *Neuroimage Clin* **1**, 121-130, doi:10.1016/j.nicl.2012.09.013 (2012).

48 Desikan, R. S. *et al.* An automated labeling system for subdividing the human cerebral cortex on MRI scans into gyral based regions of interest. *Neuroimage* **31**, 968-980, doi:10.1016/j.neuroimage.2006.01.021 (2006).

49 Jenkinson, M., Beckmann, C. F., Behrens, T. E., Woolrich, M. W. & Smith, S. M. Fsl. *Neuroimage* **62**, 782-790, doi:10.1016/j.neuroimage.2011.09.015 (2012).

50 Hawrylycz, M. J. *et al.* An anatomically comprehensive atlas of the adult human brain transcriptome. *Nature* **489**, 391-399, doi:10.1038/nature11405 (2012).

51 Hawrylycz, M. *et al.* Canonical genetic signatures of the adult human brain. *Nat Neurosci* **18**, 1832-1844, doi:10.1038/nn.4171 (2015).

52 Whitaker, K. J. *et al.* Adolescence is associated with genomically patterned consolidation of the hubs of the human brain connectome. *Proc Natl Acad Sci U S A* **113**, 9105-9110, doi:10.1073/pnas.1601745113 (2016).

53 Alexander-Bloch, A., Giedd, J. N. & Bullmore, E. Imaging structural co-variance between human brain regions. *Nature reviews. Neuroscience* **14**, 322-336, doi:10.1038/nrn3465 (2013).

54 Alexander-Bloch, A., Raznahan, A., Bullmore, E. & Giedd, J. The convergence of maturational change and structural covariance in human cortical networks. *The Journal of neuroscience : the official journal of the Society for Neuroscience* **33**, 2889-2899, doi:10.1523/JNEUROSCI.3554-12.2013 (2013).

55 Vasa, F. *et al.* Adolescent Tuning of Association Cortex in Human Structural Brain Networks. *Cereb Cortex* **28**, 281-294, doi:10.1093/cercor/bhx249 (2018).

56 Zhang, B., Kirov, S. & Snoddy, J. WebGestalt: an integrated system for exploring gene sets in various biological contexts. *Nucleic Acids Res* **33**, W741-748, doi:10.1093/nar/gki475 (2005).

57 Lake, B. B. *et al.* Integrative single-cell analysis of transcriptional and epigenetic states in the human adult brain. *Nat Biotechnol* **36**, 70-80, doi:10.1038/nbt.4038 (2018).

58 Zhu, S. *et al.* Structure of a human synaptic GABAA receptor. *Nature* **559**, 67-72, doi:10.1038/s41586-018-0255-3 (2018).

59 Wu, C. & Sun, D. GABA receptors in brain development, function, and injury. *Metab Brain Dis* **30**, 367-379, doi:10.1007/s11011-014-9560-1 (2015).

60 Fraser, D. D., Mudrick-Donnon, L. A. & MacVicar, B. A. Astrocytic GABA receptors. *Glia* **11**, 83-93, doi:10.1002/glia.440110203 (1994).

61 Traynelis, S. F. *et al.* Glutamate receptor ion channels: structure, regulation, and function. *Pharmacol Rev* **62**, 405-496, doi:10.1124/pr.109.002451 (2010).

62 Mayer, M. L. & Armstrong, N. Structure and function of glutamate receptor ion channels. *Annu Rev Physiol* **66**, 161-181, doi:10.1146/annurev.physiol.66.050802.084104 (2004).

63 Madden, D. R. The structure and function of glutamate receptor ion channels. *Nature reviews. Neuroscience* **3**, 91-101, doi:10.1038/nrn725 (2002).

64 Cornford, J. H. *et al.* Dendritic NMDA receptors in parvalbumin neurons enable strong and stable neuronal assemblies. *Elife* **8**, doi:10.7554/eLife.49872 (2019).

65 Yao, L., Grand, T., Hanson, J. E., Paoletti, P. & Zhou, Q. Higher ambient synaptic glutamate at inhibitory versus excitatory neurons differentially impacts NMDA receptor activity. *Nat Commun* **9**, 4000, doi:10.1038/s41467-018-06512-7 (2018).

66 Matute, C. Oligodendrocyte NMDA receptors: a novel therapeutic target. *Trends Mol Med* **12**, 289-292, doi:10.1016/j.molmed.2006.05.004 (2006).

67 Karadottir, R., Cavelier, P., Bergersen, L. H. & Attwell, D. NMDA receptors are expressed in oligodendrocytes and activated in ischaemia. *Nature* **438**, 1162-1166, doi:10.1038/nature04302 (2005).

68 Bajjalieh, S. M., Peterson, K., Linial, M. & Scheller, R. H. Brain contains two forms of synaptic vesicle protein 2. *Proc Natl Acad Sci U S A* **90**, 2150-2154, doi:10.1073/pnas.90.6.2150 (1993).

69 Crowder, K. M. *et al.* Abnormal neurotransmission in mice lacking synaptic vesicle protein 2A (SV2A). *Proc Natl Acad Sci U S A* **96**, 15268-15273, doi:10.1073/pnas.96.26.15268 (1999).

70 Bergles, D. E. & Richardson, W. D. Oligodendrocyte Development and Plasticity. *Cold Spring Harb Perspect Biol* **8**, a020453, doi:10.1101/cshperspect.a020453 (2015).

71 Sokoloff, L. The deoxyglucose method for the measurement of local glucose utilization and the mapping of local functional activity in the central nervous system. *International review of neurobiology* **22**, 287-333, doi:10.1016/s0074-7742(08)60296-2 (1981).

72 Magistretti, P. J. & Allaman, I. A cellular perspective on brain energy metabolism and functional imaging. *Neuron* **86**, 883-901, doi:10.1016/j.neuron.2015.03.035 (2015).

73 Pellerin, L. *et al.* Evidence supporting the existence of an activity-dependent astrocyte-neuron lactate shuttle. *Dev Neurosci* **20**, 291-299, doi:10.1159/000017324 (1998).

74 Zimmer, E. R. *et al.* [(18)F]FDG PET signal is driven by astroglial glutamate transport. *Nat Neurosci* **20**, 393-395, doi:10.1038/nn.4492 (2017).

75 Lundgaard, I. *et al.* Direct neuronal glucose uptake heralds activity-dependent increases in cerebral metabolism. *Nat Commun* **6**, 6807, doi:10.1038/ncomms7807 (2015).

76 Maschauer, S., Prante, O., Hoffmann, M., Deichen, J. T. & Kuwert, T. Characterization of 18F-FDG uptake in human endothelial cells in vitro. *J Nucl Med* **45**, 455-460 (2004).

77 Ruchti, E., Roach, P. J., DePaoli-Roach, A. A., Magistretti, P. J. & Allaman, I. Protein targeting to glycogen is a master regulator of glycogen synthesis in astrocytes. *IBRO Rep* **1**, 46-53, doi:10.1016/j.ibror.2016.10.002 (2016).

78 Sakers, K. *et al.* Astrocytes locally translate transcripts in their peripheral processes. *Proc Natl Acad Sci U S A* **114**, E3830-E3838, doi:10.1073/pnas.1617782114 (2017).

79 Regunathan, S., Feinstein, D. L. & Reis, D. J. Expression of non-adrenergic imidazoline sites in rat cerebral cortical astrocytes. *J Neurosci Res* **34**, 681-688, doi:10.1002/jnr.490340611 (1993).

80 Olmos, G., Alemany, R., Escriba, P. V. & Garcia-Sevilla, J. A. The effects of chronic imidazoline drug treatment on glial fibrillary acidic protein concentrations in rat brain. *Br J Pharmacol* **111**, 997-1002, doi:10.1111/j.1476-5381.1994.tb14842.x (1994).

81 Tesson, F. *et al.* Localization of I2-imidazoline binding sites on monoamine oxidases. *J Biol Chem* **270**, 9856-9861, doi:10.1074/jbc.270.17.9856 (1995).

82 Paterson, L. M., Tyacke, R. J., Robinson, E. S., Nutt, D. J. & Hudson, A. L. In vitro and in vivo effect of BU99006 (5-isothiocyanato-2-benzofuranyl-2-imidazoline) on I2 binding in relation to MAO: evidence for two distinct I2 binding sites. *Neuropharmacology* **52**, 395-404, doi:10.1016/j.neuropharm.2006.08.010 (2007).

83 Li, J. X. Imidazoline I2 receptors: An update. *Pharmacol Ther* **178**, 48-56, doi:10.1016/j.pharmthera.2017.03.009 (2017).

84 Keller, B. & Garcia-Sevilla, J. A. Immunodetection and subcellular distribution of imidazoline receptor proteins with three antibodies in mouse and human brains: Effects of treatments with I1- and I2-imidazoline drugs. *Journal of psychopharmacology (Oxford, England)* **29**, 996-1012, doi:10.1177/0269881115586936 (2015).

85 Arakawa, R. *et al.* Test-retest reproducibility of [(11)C]-L-deprenyl-D2 binding to MAO-B in the human brain. *EJNMMI Res* **7**, 54, doi:10.1186/s13550-017-0301-4 (2017).

86 Ekblom, J. *et al.* Monoamine oxidase-B in astrocytes. *Glia* **8**, 122-132, doi:10.1002/glia.440080208 (1993).

87 Levitt, P., Pintar, J. E. & Breakefield, X. O. Immunocytochemical demonstration of monoamine oxidase B in brain astrocytes and serotonergic neurons. *Proc Natl Acad Sci U S A* **79**, 6385-6389, doi:10.1073/pnas.79.20.6385 (1982).

88 Riederer, P. *et al.* Localization of MAO-A and MAO-B in human brain: a step in understanding the therapeutic action of L-deprenyl. *Adv Neurol* **45**, 111-118 (1987).

89 MacKay, A. L. & Laule, C. Magnetic Resonance of Myelin Water: An in vivo Marker for Myelin. *Brain Plast* **2**, 71-91, doi:10.3233/BPL-160033 (2016).

90 Sled, J. G. Modelling and interpretation of magnetization transfer imaging in the brain. *Neuroimage* **182**, 128-135, doi:10.1016/j.neuroimage.2017.11.065 (2018).

91 Schmierer, K., Scaravilli, F., Altmann, D. R., Barker, G. J. & Miller, D. H. Magnetization transfer ratio and myelin in postmortem multiple sclerosis brain. *Ann Neurol* **56**, 407-415, doi:10.1002/ana.20202 (2004).

92 Fjaer, S. *et al.* Deep gray matter demyelination detected by magnetization transfer ratio in the cuprizone model. *PLoS One* **8**, e84162, doi:10.1371/journal.pone.0084162 (2013).

93 Reeves, C. *et al.* Combined Ex Vivo 9.4T MRI and Quantitative Histopathological Study in Normal and Pathological Neocortical Resections in Focal Epilepsy. *Brain Pathol* **26**, 319-333, doi:10.1111/bpa.12298 (2016).

94 Tardif, C. L., Bedell, B. J., Eskildsen, S. F., Collins, D. L. & Pike, G. B. Quantitative magnetic resonance imaging of cortical multiple sclerosis pathology. *Mult Scler Int* **2012**, 742018, doi:10.1155/2012/742018 (2012).

95 Laule, C. *et al.* Magnetic resonance imaging of myelin. *Neurotherapeutics* **4**, 460-484, doi:10.1016/j.nurt.2007.05.004 (2007).

96 Notter, T., Coughlin, J. M., Sawa, A. & Meyer, U. Reconceptualization of translocator protein as a biomarker of neuroinflammation in psychiatry. *Mol Psychiatry* **23**, 36-47, doi:10.1038/mp.2017.232 (2018).

97 Wimberley, C. *et al.* Kinetic modeling and parameter estimation of TSPO PET imaging in the human brain. *Eur J Nucl Med Mol Imaging*, doi:10.1007/s00259-021-05248-9 (2021).

98 Gut, P., Zweckstetter, M. & Banati, R. B. Lost in translocation: the functions of the 18-kD translocator protein. *Trends in endocrinology and metabolism: TEM* **26**, 349-356, doi:10.1016/j.tem.2015.04.001 (2015).

99 Notter, T. *et al.* Neuronal activity increases translocator protein (TSPO) levels. *Mol Psychiatry*, doi:10.1038/s41380-020-0745-1 (2020).

100 Mizrahi, R. *et al.* Translocator protein (18 kDa) polymorphism (rs6971) explains in-vivo brain binding affinity of the PET radioligand [(18)F]-FEPPA. *J Cereb Blood Flow Metab* **32**, 968-972, doi:10.1038/jcbfm.2012.46 (2012).

101 Turkheimer, F. E. *et al.* The methodology of TSPO imaging with positron emission tomography. *Biochem Soc Trans* **43**, 586-592, doi:10.1042/BST20150058 (2015).

102 Hoozemans, J. J. *et al.* Cyclooxygenase expression in microglia and neurons in Alzheimer's disease and control brain. *Acta Neuropathol* **101**, 2-8, doi:10.1007/s004010000251 (2001).

103 Wu, T., Wu, H., Wang, J. & Wang, J. Expression and cellular localization of cyclooxygenases and prostaglandin E synthases in the hemorrhagic brain. *J Neuroinflammation* **8**, 22, doi:10.1186/1742-2094-8-22 (2011).

104 Garcia-Bueno, B., Serrats, J. & Sawchenko, P. E. Cerebrovascular cyclooxygenase-1 expression, regulation, and role in hypothalamic-pituitary-adrenal axis activation by inflammatory stimuli. *The Journal of neuroscience : the official journal of the Society for Neuroscience* **29**, 12970-12981, doi:10.1523/JNEUROSCI.2373-09.2009 (2009).

105 Schoenberger, M. *et al.* In Vivo [(18)F]GE-179 Brain Signal Does Not Show NMDA-Specific Modulation with Drug Challenges in Rodents and Nonhuman Primates. *ACS Chem Neurosci* **9**, 298-305, doi:10.1021/acschemneuro.7b00327 (2018).

106 Nimmerjahn, A., Kirchhoff, F. & Helmchen, F. Resting microglial cells are highly dynamic surveillants of brain parenchyma in vivo. *Science* **308**, 1314-1318, doi:10.1126/science.1110647 (2005).

107 Knudsen, G. M. *et al.* Guidelines for the content and format of PET brain data in publications and archives: A consensus paper. *J Cereb Blood Flow Metab* **40**, 1576-1585, doi:10.1177/0271678X20905433 (2020).

108 Coenen, H. H. *et al.* Consensus nomenclature rules for radiopharmaceutical chemistry - Setting the record straight. *Nucl Med Biol* **55**, v-xi, doi:10.1016/j.nucmedbio.2017.09.004 (2017).

Acknowledgments: We would like to thank all volunteers contributing data to this study.

Funding: DM, OD, MV, FT, and SCRM are supported by the NIHR Maudsley's Biomedical Research Centre at the South London and Maudsley NHS Trust. AG is supported by the KCL funded CDT in Data-Driven Health, this represents independent research part funded by the NIHR Maudsley's Biomedical Research Centre at the South London and Maudsley NHS Trust and part funded by GlaxoSmithKline (GSK). JCM received support from the Chao, Graham, Harrison, and Nantz Funds of the Houston Methodist Foundation and from the Moody Foundation.

Author contributions: DM, MV, OD and FT designed the study; DM performed the data analysis and drafted the manuscript; AG wrote the python script provided with the manuscript; all authors discussed the findings, revised the manuscript for intellectual content and approved the final version of the manuscript.

Competing interests: The authors declare no competing interests. This manuscript represents independent research.

Appendix I – PET templates references and contact points

PET Template*	Reference	Investigators	Contact point
[^{11}C]Flumazenil	[11C]-Flumazenil PET in temporal lobe epilepsy: do we need an arterial input function or kinetic modeling? *J Cereb Blood Flow Metab* **28**, 207-216, doi:10.1038/sj.jcbfm.9600515 (2008).	Alexander Hammers	Alexander Hammers, alexander.hammers@kcl.ac.uk
[^{18}F]GE179	McGinnity, C. J. *et al.* Initial evaluation of 18F-GE-179, a putative PET Tracer for activated N-methyl D-aspartate receptors. *J Nucl Med* **55**, 423-430, doi:10.2967/jnumed.113.130641 (2014).	Alex Hammers, Colm McGinnity	Colm McGinnity, colm.mcginnity@kcl.ac.uk
[^{11}C]UCBJ	n/a	Steve Williams, Chloe Farrell, Lucia Batzu, Silvia Rota, Tayyabah Yousaf, Christine A Parker, Alastair Reith	Chloe Farrell, chloe.farrell@kcl.ac.uk
[^{18}F]FDG	n/a	Bertoldo Alessandra, Erica Silvestri	Bertoldo Alessandra, bertoldo@dei.unipd.it
[^{11}C]BU99008	Tyacke, R. J. *et al.* Evaluation of (11)C-BU99008, a PET Ligand for the Imidazoline2 Binding Site in Human Brain. *J Nucl Med* **59**, 1597-1602, doi:10.2967/jnumed.118.208009 (2018).	David J Nutt, Christine Parker, Robin J Tyacke, James Myers	Robin J Tyacke, r.tyacke@imperial.ac.uk
L-[^{11}C]deprenyl-D2	Albrecht, D. S. *et al.* Brain glial activation in fibromyalgia - A multi-site positron emission tomography investigation. *Brain, behavior, and immunity* **75**, 72-83, doi:10.1016/j.bbi.2018.09.018 (2019).	Anton Forsberg, Eva Kosek, Marco Loggia	Anton Forsberg, anton.forsberg.moren@ki.se
[^{11}C]PK11195	Schubert, J. J. *et al.* A Modest Increase in (11)C-PK11195-Positron Emission Tomography TSPO Binding in Depression Is Not Associated With Serum C-Reactive Protein or Body Mass Index. *Biol Psychiatry Cogn Neurosci Neuroimaging*, doi:10.1016/j.bpsc.2020.12.017 (2021).	Julia Schubert, Ed Bullmore, NIMA consortium	Julia Schubert, julia.schubert@kcl.ac.uk
[^{18}F]DPA174	n/a	Ivana Rosenzweig	Ivana Rosenzweig, ivana.1.rosenzweig@kcl.ac.uk
[^{11}C]PBR28	Zanotti-Fregonara, P. *et al.* Head-to-head comparison of (11)C-PBR28 and (11)C-ER176 for quantification of the translocator protein in the human	Belen Pascual, Paolo Zanotti-Fregonara, Masahiro Fujita Masahiro Fujita,	Belen Pascual, BPascual@houstonmethodist.org

	brain. *Eur J Nucl Med Mol Imaging* **46**, 1822-1829, doi:10.1007/s00259-019-04349-w (2019).	Meixiang Yu, Joseph C. Masdeu	
[^{11}C]ER176	Zanotti-Fregonara, P. *et al.* Head-to-head comparison of (11)C-PBR28 and (11)C-ER176 for quantification of the translocator protein in the human brain. *Eur J Nucl Med Mol Imaging* **46**, 1822-1829, doi:10.1007/s00259-019-04349-w (2019).	Belen Pascual, Paolo Zanotti-Fregonara, Masahiro Fujita, Meixiang Yu, Joseph C. Masdeu	Belen Pascual, BPascual@houstonmethodist.org
[^{11}C]PS13	Kim, M. J. *et al.* First-in-human evaluation of [(11)C]-PS13, a novel PET radioligand, to quantify cyclooxygenase-1 in the brain. *Eur J Nucl Med Mol Imaging* **47**, 3143-3151, doi:10.1007/s00259-020-04855-2 (2020).	Paolo Zanotti-Fregonara, Robert Innis	Robert Innis, innisr@mail.nih.gov
[^{18}F]fallypride	Dunn, J., et al. "Effect of image reconstruction algorithms on binding potential calculations in [F-18]-fallypride PET." *Journal of Cerebral Blood Flow and Metabolism* 29 (2009): S4-S4.	Joel Dunn	Joel Dunn, joel.dunn@kcl.ac.uk

*Radiotracer names are written in agreement with the consensus nomenclature for radiopharmaceutical chemistry[108]

Appendix II – PET templates working group (in alphabetic order)

List of Contributors		Affiliations
Batzu	Lucia	Basic and Clinical Neuroscience, IoPPN, King's College London
Bertoldo	Alessandra	Department of Information Engineering, University of Padua, Italy; Padova Neuroscience Center, University of Padova, Padova, Italy
Bullmore	Ed R	Department of Psychiatry, School of Clinical Medicine, University of Cambridge, Cambridge, United Kingdom; Wolfson Brain Imaging Centre, University of Cambridge, Cambridge, United Kingdom
Cecchin	Diego	Nuclear Medicine Unit, Department of Medicine, University of Padova, Padova, Italy; Padova Neuroscience Center, University of Padova, Padova, Italy
Chaudhuri	Ray	Basic and Clinical Neuroscience, IoPPN, King's College London
Corbetta	Maurizio	Department of Neuroscience, University of Padova, Padova, Italy; Padova Neuroscience Center, University of Padova, Padova, Italy
Dunn	Joel	St Thomas' PET Centre at St Thomas' Hospital, King's College London
Farrell	Chloe	Centre for Neuroimaging Sciences, IoPPN, King's College London
Forsberg	Anton	Department of Clinical Neuroscience, Center for Psychiatry Research, Karolinska Institutet, and Stockholm County Council, SE-171 76 Stockholm, Sweden
Fujita	Masahiro	PET Core, Houston Methodist Research and Neurological Institutes, and Weill Cornell Medicine, 6670 Bertner Ave, Houston, TX, 77030, USA
Hammers	Alexander	St Thomas' PET Centre at St Thomas' Hospital, King's College London
Innis	Robert	Molecular Imaging Branch, National Institute of Mental Health, USA
Kosek	Eva	Department of Clinical Neuroscience, Karolinska Institutet, Sweden
Loggia	Marco	Center for Integrative Pain Neuroimaging, Athinoula A. Martinos Center for Biomedical Imaging, Harvard Medical School, US
Masdeu	Joseph C	Nantz National Alzheimer Center, Houston Methodist Neurological Institute, and Weill Cornell Medicine 6560 Fannin St, Houston, TX, 77030, USA
McGinnity	Colm	St Thomas' PET Centre at St Thomas' Hospital, King's College London
Myers	James	Neuropsychopharmacology Unit, Centre for Academic Psychiatry, Division of Brain Sciences, Faculty of Medicine, Imperial College London, UK
Nutt	David J	Neuropsychopharmacology Unit, Centre for Academic Psychiatry, Division of Brain Sciences, Faculty of Medicine, Imperial College London, UK
Parker	Christine	GlaxoSmithKline, Medicines Research Centre, Gunnels Wood Road, Hertfordshire, SG1 2NY, UK.
Pascual	Belen	Nantz National Alzheimer Center, Houston Methodist Neurological Institute, and Weill Cornell Medicine 6560 Fannin St, Houston, TX, 77030, USA
Reith	Alastair	GlaxoSmithKline, Medicines Research Centre, Gunnels Wood Road, Hertfordshire, SG1 2NY, UK.
Rosenzweig	Ivana	Sleep and Brain Plasticity Centre, Department of Neuroimaging, IoPPN, King's College London
Rota	Silvia	Centre for Neuroimaging Sciences, IoPPN, King's College London
Schubert	Julia	Centre for Neuroimaging Sciences, IoPPN, King's College London
Silvestri	Erica	Department of Information Engineering, University of Padua, Italy; Padova Neuroscience Center, University of Padova, Padova, Italy
Suarez Contreras	Vanessa	Centre for Neuroimaging Sciences, IoPPN, King's College London
Tyacke	Robin J	Neuropsychopharmacology Unit, Centre for Academic Psychiatry, Division of Brain Sciences, Faculty of Medicine, Imperial College London, UK
Williams	Steve	Centre for Neuroimaging Sciences, IoPPN, King's College London
Yousaf	Taytayyabah	Centre for Neuroimaging Sciences, IoPPN, King's College London
Yu	Meixiang	Cyclotron and Radiochemistry Core, Houston Methodist Research Neurological Institute, and Weill Cornell Medicine, 6670 Bertner Ave, Houston, TX, 77030, USA
Zanotti-Fregonara	Paolo	Molecular Imaging Branch, National Institute of Mental Health, USA